Lymphoscintigraphy is more effective using higher specific activity ^{99m}Tc-antimony trisulfide colloid in the rat

Abstract

Technetium-99m-antimony trisulfide colloid (^{99m}Tc-ATC) was investigated with varying specific activity in the rat lymphatic system, as well as its binding to rat blood cells *in vitro*. Low, moderate and high doses of ^{99m}Tc-ATC were subdermally injected into tails of rats (n=3) and 30min later whole body lymphoscintigraphic images were acquired. ^{99m}Tc-ATC was incubated for 30min at 37˚C with whole blood (n=4) as for control, at 4˚C as for hypothermia, as opsonized at 37˚C and lipopolysaccharide (LPS) at 37˚C. Cell types were separated by gradient centrifugation to assay for cell bound-radioactivity. These experiments were repeated using mixed leukocytes that were erythrocytes-free. Images showed direct drainage of ^{99m}Tc-ATC from the tail to the popliteal nodes, sacral node and beyond, along the para-aortic chain, and to a left inguinal lymph node that drained into the axillia. The higher specific activity dose resulted in more visible lymph nodes after 30min. ^{99m}Tc-ATC was predominantly not cell-bound. In rat whole blood ^{99m}Tc-ATC-neutrophils were only present to the extent of 3% for the control, 3% for the hypothermia test, 4% for the opsonized and 7% for the LPS test. In the erythrocytes-free samples, ^{99m}Tc-ATC-leukocytes were present to the extent of 5% (control), 4% (hypothermia), 6% (opsonized) and 11% (LPS). *In conclusion*, a higher specific activity radiocolloid may identify the sentinel lymph node sooner during lymphoscintigraphy, and there may be an advantage in detecting more counts with the γ-probe. Retention of ^{99m}Tc-ATC in lymph nodes *in vivo* is likely because of binding on macrophage surfaces, rather than from internalization by phagocytosis within a time frame of 30min after injection.

Hell J Nucl Med 2014; 17(1): 19-26 *Published online: 27 March 2014*

Chris Tsopelas PhD

Royal Adelaide Hospital Radiopharmacy, Nuclear Medicine Department, North Terrace, Adelaide, Australia, 5000

Keywords: Lymphoscintigraphy
- ^{99m}Tc-antimony trisulfide colloid
- Rats
- Specific activity radiopharmaceutical
- In vitro cell binding

Correspondence address:
Dr Chris Tsopelas,
RAH Radiopharmacy,
Royal Adelaide Hospital,
Nuclear Medicine Department, North Terrace,
Adelaide, Australia, 5000.
Facsimile number: + 61 8 8222 4370
Email: ctsopela@mail.rah.sa.gov.au

Received:
4 March 2014
Accepted:
10 March 2014

Introduction

Lymphoscintigraphy is a routine technique performed in the Nuclear Medicine clinic for mapping the lymphatic system that drains the primary tumour, employed to identify the sentinel lymph node(s) and potentially harbouring metastatic cells. Successful radiopharmaceutical colloids used for this indication include technetium-99m-antimony trisulfide (^{99m}Tc-ATC) [1], ^{99m}Tc-tin fluoride [2-4], ^{99m}Tc-sulfur [5], ^{99m}Tc-human-albumin [6] and ^{99m}Tc-rhenium sulfide [7]. Radiotracer is usually administered to the patient intradermally over a number of sites around the tumour, and particularly for the small colloids, accumulating radioactivity is detected in the sentinel node(s) during the acquisition of a scan within the next ~30min. From the scan information, the skin is marked with a pen at the location corresponding with a concentration of gamma counts. The patient is then taken to theatre where a coloured dye (usually blue, or green) is given, and this provides a visual signal simultaneously with the radioactive signal, to aid the surgeon during an operation in localizing the node. The sentinel node biopsy procedure involves harvesting a small sample of the lymph node with its efferent and afferent channels, for rapid histological assessment *in situ*. If the nodal status is negative for tumour cells the surgeon completes the simple procedure, a positive result would otherwise incur a more invasive wide local excision in which the patient may later experience a complication of secondary lymphedema.

In terms of the physiological process after intradermal injection of radiocolloid, particles are deposited at the interstitial cellular matrix and then they diffuse toward the lymphatic capillaries before contact with lymph. The smaller radiocolloid particles enter the lymphatic lumen quickly and easily, although larger particles may be excluded from passively crossing the lymphatic endothelial cell barrier. Protein-rich lymph carries particles toward the impending lymph node, the flow rate does vary according to location in the body, and depends mainly upon muscular activity, temperature or occlusion by tumour deposits [8]. Particles retained within the lymph node parenchyma, are generally accepted to result from phagocytic engulfment by neutrophils, monocytes [9] and eosinophils [10]. It is unclear to what extent phagocytosis occurs within the acquisition

time of a scan, nevertheless there is sufficient detectable radioactive signal to visualize lymph nodes.

The commercial radiocolloids are listed in Table 1, these are easily prepared in the radiopharmacy and a final product formulation can be made available for injection on-site within 3-60min. Each manufacturer-recommended procedure requires the operator to reconstitute a cold kit with a broad ^{99m}Tc-pertechnetate concentration range, in a step that impacts on the final radioactive concentration and specific activity of the product. Radioactive concentration is defined as the amount of radioactive material (MBq) per volume (mL) of liquid, and does not consider the quantity of cold material present. In contrast, specific activity is defined as the amount of radioactive material per unit mass of the element or the cold material concerned. In the case of a radiocolloid particle, the monomer formula is typically chosen for the calculation. If the molecular weight of the cold compound is known, then specific activity is stated in MBq per moles. For lymphoscintigraphy, a total injected dose of 5-30MBq is considered sufficient when same day breast cancer surgery [11] is planned, and preferably when it is administered as a bolus volume [12]. Each dose contains a mixture of ^{99m}Tc-particles and non-radioactive particles, the latter are always present in excess [13]. Specific activity is a parameter that considers the amount of cold material present, and when this material is in the form of particles, it is especially important at the cellular level if the total particle population exceeds the number of lymph node macrophages. It was previously reported for antimony trisulfide that there are an estimated $5x10^{13}$ cold particles per mL of cold kit formulation [14]. Technetium-99m-ATC was chosen as the radiotracer for this study, for the purpose of investigating the effect of specific activity on the quality of rat lymphoscintigrams, to explore its binding affinity with leukocytes in vitro, and to better understand the immune events occurring at the cellular level *in vivo*.

Materials and methods

Technetium-99m-pertechnetate was obtained from the eluent of a dry-bed ^{99}Mo/^{99m}Tc-generator (Gentech; Australian Radioisotopes; Sydney; Australia). Normal saline (0.9%) injection was used for dilutions and washes. Histopaque gradient solutions and LPS (*E. coli*) were purchased from Sigma-Aldrich (St. Louis; USA). All measurements of radioactivity in the calibrated dose calibrator unit (Atomlab 100+ Dose Calibrator; Biodex Medical Systems; New York; USA) were background corrected. All *in vivo* experiments were performed in triplicate, and the *in vitro* blood experiments (n=4) were performed at 37.0±0.5˚C using a heated water bath (TECAM; Techne; Cambridge; England), except for the hypothermic condition (ice-water bath at 0-4˚C). Radioactive blood containers were shaken (80rpm) during heating, using a platform mixer (OM6; Ratek; Victoria; Australia) located next to the water bath that connected a configuration of boss heads and clamps.

Radiolabeling procedures

Preparation of ^{99m}Tc colloidal antimony sulfide injection

Lymph-Flo kit (RAH Radiopharmacy; Adelaide; Australia) consisted of five separate non-radioactive components: antimony trisulfide (AT); phosphate buffer (PB); hydrochloric acid (HA); an empty sterile 10mL vial; a sterile 0.2μm filter. The procedure for preparing radiocolloid included adding ^{99m}Tc-pertechnetate (240MBq/0.4mL saline) and then HA (1.0 M; 0.1mL) to the vial containing AT (1mL). This reaction vial was heated at 100˚C for 30min, allowed to cool to room temperature, and then neutralized with PB (0.5mL). The formulation was filtered into the empty vial. From this vial, a dose (0.04mL; 4.8MBq) of 'low' specific activity (0.08GBq/μmol) was withdrawn using an insulin syringe (0.5mL; Becton Dickinson & Co; Singapore). A dose (0.04mL; 4.8MBq) of "moderate" specific activity (0.77GBq/μmol) was obtained from a ^{99m}Tc-ATC vial, reconstituted with ^{99m}Tc-pertechnetate (2400MBq/0.4mL saline) and finally diluted 1:10 in saline (0.9mL). The "high"specific activity dose (7.69GBq/μmol) was prepared differently. An aliquot (0.1mL) from an AT vial was diluted with saline (0.9mL) in an air-filled vial, then the orange dispersion was reconstituted with ^{99m}Tc-pertechnetate (2.40GBq/0.2mL saline) and HA (1.0 M; 0.05mL). This reaction vial was treated as above and then neutralized with PB (0.25mL) prior to filtration. The formulation was diluted 1:10 in saline, a dose (0.03mL; 4.8MBq) was withdrawn and then further diluted with saline (to 0.04mL) prior to use.

Radiochemical analyses

Radiochemical purity was determined by ascending instant thin layer chromatography with silica gel impregnated glass

Table 1. *Criteria to prepare common lymphoscintigraphic tracers*

Name		^{99m}Tc-pertechnetate concentration (MBq/mL)	Final ^{99m}Tc-colloid formulation			Cold material
Cold kit	^{99m}Tc-colloid		Volume (mL)	Concentration (MBq/mL)	Specific activity (MBq/μg cold)	
Lymph Flo kit	antimony trisulfide	800-900	2.6	291-327	0.7-0.8	Sb_2S_3*
Leucocyte labelling kit	tin fluoride	500-800	3.0	445-593	21-28	SnF_2**
Amerscan hepatate	tin fluoride	1-18500	4.0	0.25-4546	0.01-28	SnF_2**
Sulfur colloid	sulfur	185-5550	1.0	175-5239	0.001-9.1	thiosulfate**
Nanocoll	human albumin	0.3-1233	3.0	0.32-1184	0.3-10.5	albumin**
NanoCIS	rhenium sulfide	370-5550	2.5	140-2095	1.5-22	Re_2S_7*

** known formula comprising the particle matrix; ** product formula unknown, specific activity based on the starting material*

fibre strips (1x16cm; Gelman Sciences; Michigan; USA) developed in saline (0.9%), to determine the level of ^{99m}Tc-pertechnetate that migrated with the solvent front. The strip sections were counted in a gamma counter (Cobra II Auto-Gamma; Canberra Packard; Victoria; Australia) over a ^{99m}Tc window (90-190keV). The manufacturer limit for % radiochemical purity of ^{99m}Tc-ATC injection was >95% and with specific activity of 0.24-0.27 GBq/μmol.

Animal studies

Experiments performed with rats complied with "*The Australian Code of Practice for the Care and Use of Animals for Scientific Purposes NHMRC*" and according to a protocol approved by the Animal Ethics Committee of the Institute of Medical and Veterinary Science, Adelaide, South Australia. Samples of 10mL of whole blood were obtained from rats (Sprague-Dawley; 200g) by intra-cardiac puncture using a syringe containing 60 units of heparin in 0.6mL of saline. Plasma for the opsonization experiments was obtained by centrifuging heparinised rat blood at 100g for 20min, then in a sterile vial the rat plasma (4mL) was added to ^{99m}Tc-ATC (1mL; 1000MBq) and mixed to form a homogeneous dispersion. The vial was allowed to stand at room temperature for 10min and opsonized radiocolloid was used immediately in the cell binding studies. Cells incubated at 37˚C *in vitro* represented the physiological body temperature.

Scintigraphic imaging

Nine female rats (Sprague-Dawley; 150g) were injected subdermally in the tail with ^{99m}Tc-ATC (4.8MBq; 0.04mL) using an insulin syringe (0.5mL BD Ultra-Fine; Becton Dickinson; USA). At 30min they were sacrificed and then five minute whole body static images were acquired using a gamma camera (Starcam or MPR; GE Medical Systems; Wisconsin; USA). Regions of interest (ROI) analyses were performed on each image using counts of the (left plus right) popliteal nodes and the sacral node. The % lymph node uptake was calculated by dividing the lymph node counts by the total counts and multiplied by 100. All values were background corrected.

Distribution of ^{99m}Tc-ATC in rat blood cells

Isolation of leukocytes. To each of four polystyrene tubes (13x85mm; Sarstedt; Germany) was added a centrifugation gradient solution (Histopaque-1119; 6.0mL; density=1.119g/mL), and then a second gradient solution (Histopaque-1077; 6.8mL; density=1.077g/mL) was carefully layered on top to avoid mixing. Non-radioactive heparinised rat whole blood (2.5mL) was added onto the top gradient layer taking care not to disrupt the liquid interfaces. This procedure was repeated another three times, each of the four centrifuge tubes were secured in custom supports within buckets of a centrifuge (Cellsep 6/720R; Sanyo Gallenkamp PLC; Loughborough, UK), and then spun at 750g for 18min at 22˚C. The leukocyte and plasma layers were harvested from the red cell pellet, the combined volume (~10mL) was used for the cell binding experiments.

Radiocolloid incubated with blood cells. The ^{99m}Tc-ATC was prepared with ^{99m}Tc-pertechnetate (420MBq/0.4mL saline), AT (1mL), HA (1.0 M; 0.1mL), a heating step then neutralization with PB (0.5mL) as above. The general incubation procedure involved an addition of ^{99m}Tc-ATC (0.2mL; 35MBq; 4x10^{12} ATC particles) to rat whole blood or isolated rat leukocytes (10mL), and the fluid was kept at 37˚C for 30min (control). Three variations of this procedure were performed for whole blood: (i) opsonized-^{99m}Tc-ATC (1.0mL; 30MBq) replaced ^{99m}Tc-ATC; (ii) the peripheral blood sample and radiocolloid were both chilled in ice water to 0-4ºC for 3min prior to their combination, then the fluid was kept at 4ºC for 30min; and (iii) the peripheral blood sample was pre-treated for 2min at room temperature with lipopolysaccharide (LPS) in saline (13.4μg/mL; 0.26mL). Also, three other variations of the procedure were performed using leukocytes with: (i) opsonized-^{99m}Tc-ATC; (ii) hypothermia condition; and the (iii) LPS condition.

Separation of radioactive samples

Each radioactive sample (4x2.5mL) was carefully added onto a top gradient layer of the two-gradient centrifugation solution as above. The four samples were spun at 750g for 18min at 22˚C (or 4˚C for hypothermia). Every layer per tube was isolated using an insulin syringe (0.5mL; Becton Dickinson; Singapore) and then counted in the dose calibrator. The distribution of radiocolloid in each tube was calculated as the percentage of activity in a layer relative to the total activity.

Statistical analyses

Results are expressed as mean ± standard error (SE). Statistical analyses with paired sample t-tests compared the: (i) different ^{99m}Tc-ATC specific activities for left plus right popliteal nodes; (ii) different ^{99m}Tc-ATC specific activities for sacral nodes; (iii) popliteal nodes versus sacral node (low specific activity); (iv) % radiocolloid bound to neutrophils at 37˚C (control), versus 0-4˚C, versus opsonized-^{99m}Tc-ATC; or versus LPS; and (v) % radiocolloid bound to leukocytes at 37˚C (control), versus 0-4˚C, versus opsonized-^{99m}Tc-ATC; or versus LPS. Statistical significance was defined as a P value less than 0.05. The sample size/number of experiments that generated parametric data was sufficient for statistical analyses.

Results

Radiochemical analysis and biodistribution

Radiochemical purity of ^{99m}Tc-ATC was found to be 98.0±0.4% for low to high specific activity kits (n=4). The scintigraphic images at 30min after ^{99m}Tc-ATC injection in rat tail are shown in Figure 1 and the ROI data is summarised in Table 2 as per specific activity dose.

After injection of ^{99m}Tc-ATC in rat tails, the radiotracer migrated in lymph to both left and right popliteal nodes, onto a common sacral node and then drained further into the cisternal lymph node. Particularly for the high specific activity dose, an inguinal node and auxiliary lymph node were also visible. The scans showed low level of liver, spleen and bone marrow uptake, typical of radiocolloid distribution in the mammalian reticuloendothelial system [8]. The scan of low specific activity ^{99m}Tc-ATC displayed less lymphatic drainage information than the moderate or high specific activity ^{99m}Tc-ATC scans, attributable to the relatively lower ^{99m}Tc signal. All 9/9 rats had the same lymphatic anatomy, more nodes were visible when high specific activity radiocolloid was used (6 nodes) than moderate specific activity (4 nodes) or low spe-

cific activity (3 nodes). This was also emphasized by the ROI analysis of two popliteal nodes per scan, as the specific activity of the dose increased, uptake by the popliteal node pair significantly increased. The sacral node uptake remained the same irrespective of the specific activity of ^{99m}Tc-ATC dose. Different sized popliteal nodes seen on all scans (3/3 in Fig. 1) indicated one of the two lymphatic vessels was more dominant. Lymphatic pathways were clearly visible from tail to the upper trunk in the high specific activity image, and the multiple number of nodes suggested more than one drainage route from the tail.

^{99m}Tc-ATC binding to rat blood cells in vitro

Whole blood. After sedimentation of the radioactive samples, four distinct bands or layers were visible in the tubes. The top layer was identified as the plasma (1.5mL), the second layer included mononuclear lymphocytes (0.5mL), followed by a distinct third layer of neutrophils (1.0mL), and the red cells comprised the bottom layer (3.0mL) [15, 16]. For the control condition where non-opsonized particles were administered, most of the activity (70%) was identified in the plasma after 30min at 37˚C, it was not cell bound (Table 3). Technetium-99m-ATC was bound to lymphocytes, platelets and red cells that totalled ~30%. Three percent of radiocolloid was associated with the neutrophils. At the cold temperature, there was less red cell-associated radiocolloid activity and ~9% more plasma activity. The % radiocolloid bound to neutrophils under the control condition, was not significantly different to that of the hypothermia condition.

Partially opsonized ^{99m}Tc-ATC incubated in whole blood for 30min resulted in a similar distribution profile as the hypothermia condition, with 77% unbound radiocolloid in the plasma, 17% binding to red cells, 2% binding to lymphocytes and platelets, however there was significantly more ^{99m}Tc-ATC-bound to neutrophils than at 4˚C or 37˚C (non-opsonized control). In the presence of LPS, significantly higher ^{99m}Tc-ATC was associated with neutrophils, the other cells and plasma had a similar distribution profile to the control condition.

Leukocytes. Red cells were easily removed from the whole blood sample by gradient centrifugation, then the plasma leukocytes were used in the radiocolloid binding experiments. After sedimentation of the radioactive samples, three distinct layers were visible in the tubes. The top layer was identified as the plasma (2.7mL), the second layer included leukocytes (1.1mL), and the gradient medium comprised the bottom layer (2.0mL) [15, 16]. For the control condition where non-opsonized particles were used, almost all of the radioactivity (94%) after 30min at 37˚C was not cell bound (Table 4). Technetium-99m-ATC was bound to leukocytes to an extent of ~5%. At the cold temperature, the same distribution profile was obtained versus the control condition. Opsonized ^{99m}Tc-ATC resulted in significantly more binding (24%) to leukocytes, and there was even higher binding (2.4x) of non-opsonized ^{99m}Tc-ATC in the presence of LPS, versus the control condition.

Discussion

This study of the lymphatic system investigated the effect of specific activity of ^{99m}Tc-ATC on the quality of rat images and characterized the radiocolloid-blood cell interaction for elucidation of the binding mechanism in lymph nodes. The results are discussed in two parts, of lymphatic flow at the

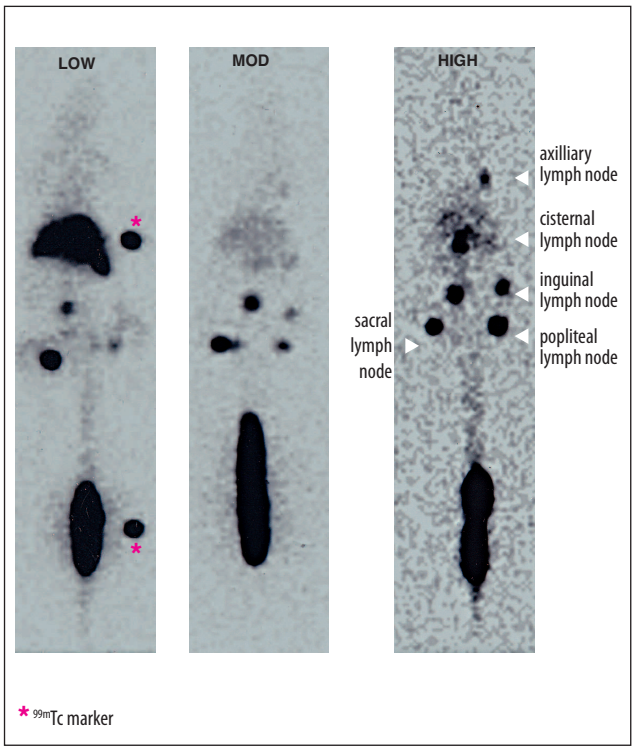

Figure 1. Anterior rat images at 30min after subdermal tail injection of low, moderate and high specific activity ^{99m}Tc-ATC doses.

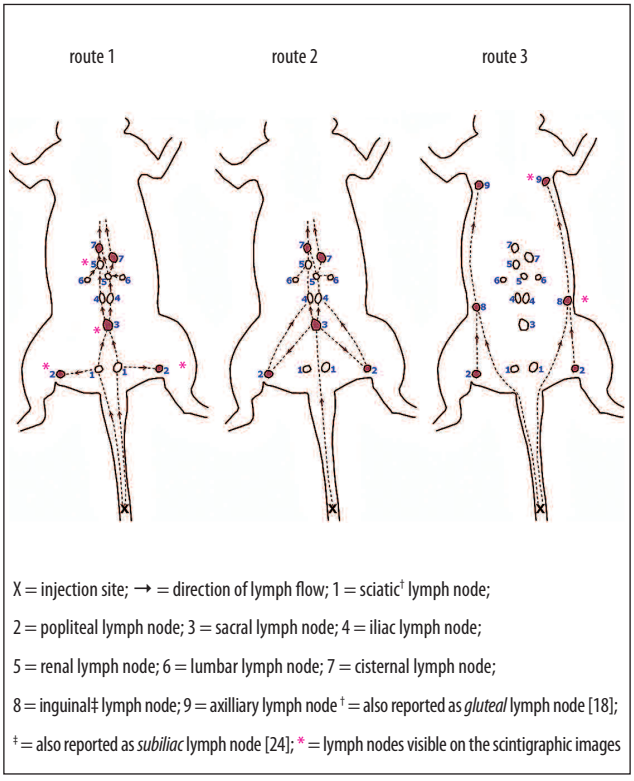

Figure 2. *Diagrams summarizing major lymphatic drainage routes from rat tail.*

physiological level, as well as the radioantigen interaction with leukocytes at the cellular level.

Lymphatic flow of ^{99m}Tc-ATC at the physiological level

Technetium-99m-ATC doses with the same radioactive concentration (4.8MBq/0.04mL) were subdermally administered into the mid-tail of rats, the bolus volume was chosen to minimize any local hydrostatic pressure on the interstitial cell matrix and the initial lymphatic sacs [17]. Lymph drainage from the rat tail followed three routes, consistent with reports in the literature [18-22]. The lymphatic anatomy in the hind quarters of a rat can vary within-species in which one or both sciatic nodes are absent [22], and between-species in particular for the mesenteric nodes [23], however the gross anatomy has been well documented [24]. Each of the three routes are summarized below with the aid of annotated diagrams (Fig. 2).

In the first route, drainage from the tail occurs along the caudal channels into the sciatic foramen to one or both of the sciatic nodes. Minor efferent trunks from each sciatic node drain to the nearest popliteal node, major trunks drain to the sacral node, onto the iliac nodes and then to the respective renal nodes. Retroperitoneal nodes (ie: lumbar) drain into the renal nodes. Efferent lymph from the right renal node flows to the right cisternal node, and the left renal node may empty into the cisternal chili directly, but more frequently an efferent lymph trunk runs across the great vessels to join the right renal node [18]. The cisternal group of nodes are contiguously linked with other para-aortic lymph nodes in the thorax. The second route involves lymph drainage along an efferent trunk from the tail to the sacral node, and beyond into the para-aortic chain as per route 1. The sacral node is an important lymph node in the pelvic region, because it has minor efferent trunks to both popliteal nodes which serve as a secondary drainage site for the tail, as well as to the large iliac nodes that are usually present as pairs. The iliac nodes are important drainage sites for popliteal nodes. The third route concerns other vessels from the tail that course laterally across the groin to the inguinal nodes. The large efferent inguinal lymphatic trunk courses caephalad along each nipple line to the axilliary node in the axilla, consistently seen in rats and mice [19]. Smaller tributary vessels from the popliteal nodes are also connected to the inguinal nodes.

In this study, the 30min images of Sprague-Dawley rats in Figure 1 showed direct drainage of ^{99m}Tc-ATC from the tail to the popliteal nodes in absentia of any sciatic nodes, then to the sacral node and beyond along the para-aortic chain, but also to the left inguinal lymph node that drained onto the axilliary node. The low specific activity ^{99m}Tc-ATC image showed left and right popliteal nodes plus the sacral node (3 nodes), the moderate specific activity image also showed the inguinal node (4 nodes) and a possible faint node in the axilla. The high specific activity ^{99m}Tc-ATC dose resulted in the visualization of all of these lymph nodes, the axilliary node was clearly distinguishable, and the low liver uptake permit-

***Table 2**. Lymph node uptake of ^{99m}Tc-ATC (4.8MBq) with altered specific activity*

Type	% injected dose (mean±SE) of specific activity ^{99m}Tc-ATC		
	0.08 GBq/μmol (low)	0.77 GBq/μmol (moderate)	7.69 GBq/μmol (high)
Popliteal nodes (R+L)[a]	1.18±0.13%	2.06±0.19%	3.60±0.19%
Sacral node[b]	0.54±0.05%	0.48±0.04%	0.54±0.19%
# ATC particles in dose	$1x10^{12}$	$1x10^{11}$	$1x10^{10}$

a: low versus moderate P=0.02, low versus high P=0.01, moderate versus high P=0.04; b: low versus moderate P=0.26, low versus high P=0.50, moderate versus high P=0.40; a versus b: P=0.03

***Table 3**. Effect of hypothermia, opsonization and LPS-activation on the fate of ^{99m}Tc-ATC incubated with rat whole blood in vitro*

Type	% radiocolloid distribution (mean±SE) under the experimental condition			
Layer	Control[a]	Hypothermia[b]	Opsonized particles[a]	LPS[a]
Plasma	69.5±0.9	78.1±0.2	76.9±0.2	69.3±0.4
Lymphocytes + platelets	2.8±0.2	2.2±0.1	2.1±0.1	3.1±0.3
Neutrophils[c]	2.5±0.1	2.8±0.1	4.0±0.0	6.7±0.0
Red cells	25.3±1.1	17.0±0.1	16.9±0.2	20.9±0.1
Sample size	n=4	n=4	n=4	n=4

a: 37°C/30min; b: 0-4°C/30min; c: hypothermia versus control P=0.06, opsonized versus control P<0.01, LPS versus control P<0.01

***Table 4**. Effect of hypothermia, opsonization and LPS-activation on the fate of ^{99m}Tc-ATC incubated with rat mixed-leukocytes in vitro*

Centrifugation	% radiocolloid distribution (mean±SE) under the experimental condition			
Layer	Control[a]	Hypothermia[b]	Opsonized particles[a]	LPS[a]
Plasma	94.0±0.1	95.2±0.3	93.3±0.2	87.6±0.5
Leukocytes[c]	4.6±0.1	4.3±0.2	5.7±0.2	11.2±0.3
Gradient medium	0.2±0.0	0.1±0.0	0.2±0.0	0.4±0.3
Sample size	n=4	n=4	n=4	n=4

a: 37°C/30min; b: 0-4°C/30min; c: hypothermia versus control P=0.17, opsonized versus control P<0.01, LPS versus control P<0.01

ted a discrete yet identifiable cisternal lymph node (6 nodes). The principal uptake by popliteal nodes was assumed to be via route 1, despite the minor drainage path of lymph from the sacral node. With an increasing specific activity ^{99m}Tc-ATC dose, the ROI image analysis of left plus right popliteal nodes also significantly increased (1.2% for low, 2.1% for moderate, 3.6% for high), yet the sacral node remained unchanged (0.5% for low, moderate and high). The number of particles per dose shown in Table 1 were based on the reported number of particles per cold kit [14]. The high specific activity ^{99m}Tc-ATC dose contained more radioactive particles among the cold particle population (versus moderate and low), and in the presence of a cellular retention mechanism more radioactive particles were retained in the simple lymph node architecture (ie: efferent flow approximately equal to afferent lymph flow). The sacral node is a major draining node for the hind quarters of the rat, its complex architecture is likely to have multiple efferent and afferent channels, and the higher throughput of lymph may explain the same ^{99m}Tc-ATC uptake between the three specific activity doses. Also visible in 9/9 images was more intense uptake in one of two popliteal nodes per rat, an observation that concurs with another in female Sprague-Dawley rats describing the presence of one dominant vessel and another non-dominant vessel in the tail [25].

The scans also showed low levels of liver, spleen and bone marrow uptake, typical of radiocolloid distribution in the mammalian reticuloendothelial system. Uptake by these organs after 30min is most likely due to radiocolloid entry into the blood circulation via fine capillaries in the tail, and perhaps to a lesser extent also via the primo vascular system inside lymphatic vessels [20], or via the thoracic duct in which lymph drains into the subclavian vein.

Radiocolloid-antigen interaction with blood cells

The chemical structure of antimony trisulfide can exist as a tetramer cage molecule (Sb_4S_6), although the more common form is a polymeric ribbon-like lattice comprised of interlocking SbS_3 and Sb_3S units, that has a nominal monomer formula of Sb_2S_3 [26]. Akin to the structure of arsenic trisulfide, antimony trisulfide colloidal particles also contain an electrical double layer comprising an excess of thiol and sulfide groups at the surface [27]. Few ^{99m}Tc-atoms are chelated onto an ATC particle [13] yet the outer layer of numerous thiol groups can bind to blood cell surfaces, in the presence or absence of opsonic molecules. Under the experimental conditions of this study, ^{99m}Tc-ATC mainly (≈75%) did not bind to blood cells. The dominant number of erythrocytes in the total cell sample did bind more radiocolloid, in contrast to the fewer number of leukocytes present. The neutrophils were conveniently isolated from the other cells in whole blood, a phenotype that is capable of internalizing radiocolloid-antigen. This was explored by comparing radiocolloid binding to neutrophils at 37˚C (control) versus 4˚C (hypothermia). Under both temperature conditions the same value of 3% radioactivity was associated with neutrophils. It has been shown that neutrophils do not phagocytose antigen-cargo at 4˚C [28-31]. Hypothermia allows antigen binding via Lyn-tyrosine kinase accumulation between the cell surface and the particle, but particle internalization is blocked [32] because there is an inhibition of actin dynamics or cytoskeletal changes necessary for probing and/or engulfment [33]. The same level of ^{99m}Tc-ATC-leukocytes detected at 4˚C and 37˚C, indicates radiocolloid is surface-bound to these cells *in vitro*.

When the radio-antigen was opsonized with complement proteins, there was significantly higher uptake by neutrophils, indicating that opsonic molecules enhance surface attachment. The opsonins C3b and C4b are known to bind with foreign material via a transthioesterification reaction [34]. These surface bound molecules may also bind to local immunoglobulins containing Fcγ moiety, or the germline antibodies can bind directly to antigen particles. Macrophages recognize such signals via their C3aR, C5aR/FcγR (I/III or IIB) receptors, and this binding reaction with opsonins defines the surface attachment of antigen. Conformational changes on the exterior cell surface ensue, signals are transmitted inward to the cytoplasm and this ultimately results in actin remodeling, phagosome formation, degranulation and cytokine signaling [35]. Phagocytic cells can also bind directly to antigen via pattern recognition receptors such as CD14 [36], C-type lectin receptors [37], dectin-1 [38] and macrophage receptor with collagenous structure, MARCO [39]. The widely studied plasma membrane-localized-CD14 binds with antigens such as bacterial cell debris (ie: LPS), or endogenous molecules (ie: ICAM-3) on the surface of apoptotic cells. It is a critical entity in signaling toll-like receptor 4, a Syk/PLCγ2-mediated endocytosis forms a loaded endosome that can initiate gene transcription of pro-inflammatory interferons such as IFN-γ [36]. Macrophages activated by IFN-γ display increased receptor mediated phagocytosis [40]. The phagocytic pathway commences when the ligand-receptor at the cell surface triggers remodeling of the actin cytoskeleton, then a phagocytic cup forms around the particle, and eventually the membrane morphologically envelopes it in a sequence of steps via the *zipper mechanism* [41].

LPS is the principal component of the outer membrane of Gram-negative bacteria, and is a *pathogen associated molecular pattern* recognised by the"polyspecific" receptor CD14 [42]. This potent immunostimulant consists of a lipophilic membrane anchor (ie: lipid A from *E. coli*) bonded on one end to a non-repeating oligosaccharide core, and a polysaccharide component (O-antigen) attached on the other end of the sugar chain to terminus [43]. LPS-activated CD14 results in up-regulated phagocytosis of antigen by macrophages via toll like receptor signaling [44]. In this study, LPS-primed neutrophils were associated with a higher uptake of ^{99m}Tc-ATC, although it was not clear if this increase was due to increased surface binding or increased phagocytosis, or both, over the experimental time frame.

The difficulties in isolating a practical volume of rat lymph were avoided by using plasma leukocytes. These mixed leukocytes were efficiently separated from erythrocytes by the gradient centrifugation technique and used as a mimic of lymph. A low 4% radiocolloid-leukocytes at 4˚C represented the level of surface attachment after 30min, 5% at 37˚C suggested there may be some internalization at the physiological temperature. As observed with the whole blood experiments, opsonization and LPS-primed leukocytes resulted in significantly higher uptake of ^{99m}Tc-ATC particles by leukocytes.

In summary, after subdermal injection of ^{99m}Tc-ATC in the rat tail, the particles delivered to interstitial tissue are likely to be partially opsonized during their migration from the injection site, and in lymph. The stream of opsonized and non-opsonized particles is propelled in lymph flowing to the first draining node (ie: sacral), where macrophages located at the subcapsular and medullary sinuses actively extract radiocolloid particles. When there is a higher ratio of radioactive particles to cold particles in the dose, a higher ^{99m}Tc-signal is bound to local macrophages and readily detectable. Nevertheless, excess radiocolloid particles percolate past the macrophages and continue with efferent lymph onto the next contiguously linked lymph nodes (ie: cisternal). At 30min after injection, visible radioactive lymph nodes on the scans are primarily due to a retention mechanism of ^{99m}Tc-ATC particles attached to macrophage surfaces at the expense of little or no internalization. The moderate to higher specific activity doses (0.8-7.7GBq/μmol) yielded more diagnostic information on the scans, a potential advantage over the clinical formulation (0.2-0.3GBq/μmol), because the enriched ^{99m}Tc-signal allowed the visualization of immune complexes at higher tier lymph nodes in the chain.

Conclusion

Based on the results from this pre-clinical rat study, higher specific activity ^{99m}Tc-ATC radiopharmaceutical may prove beneficial in a clinical setting when a high concentration of lymph node counts during lymphoscintigraphy more confidently identifies the sentinel node sooner, or discerns more complex drainage paths. More radioactive counts in the target organ may also provide an advantage to the surgeon during detection with the γ-probe in the surgical theatre. Retention of ^{99m}Tc-ATC in lymph nodes is unlikely to involve macrophage internalization within 30min after injection, however radiocolloid attachment to the surface of resident cells does explain the retention mechanism *in vivo*.

Bibliography

1. Lymph Flo Kit, Product Insert. *RAH Radiopharmacy*, Australia.
2. Tin Colloid, Product Insert. *Nihon Medi-Physics*, Japan.
3. Labelling Leukocyte Kit (Stannous Colloid), Product Insert. *Radpharm Scientific*, Australia.
4. Amerscan Hepatate, Product Insert. *GE Healthcare*, United Kingdom.
5. Kit for the Preparation of Technetium Tc-99m Sulfur Colloid Injection, Product Insert. *Pharmalucence*, USA.
6. Nanocoll, Product Insert, *GE Healthcare*, Italy.
7. NANOCIS, Product Insert. *IBA*, France.
8. Tsopelas C, Munns SL, Daniels CB et al. Biodistribution and lymphatic speed of ^{99m}Tc-antimony trisulphide colloid in the lizard *Pogona Vitticeps*. *Hell J Nucl Med* 2002; 1: 42-5.
9. Ikomi F, Hanna GK, Schmid-Schönbein GW. Mechanism of colloidal particle uptake into the lymphatic system: basic study with percutaneous lymphography. *Radiology* 1995; 196: 107-13.
10. Munz DL, Senekowitsch R, Sessler MJ et al. Uptake mechanism of interstitially injected ^{99m}Tc-labeled antimony trisulphide colloid in the popliteal lymph node of rabbits. *Nuklearmedizin* 1985; 24: 39-43.
11. Giammarile F, Alazraki N, Aarsvold JN et al. The EANM and SNMMI practice guideline for lymphoscintigraphy and sentinel node localization in breast cancer. *Eur J Nucl Med Mol Imaging* 2013; 40: 1932-47.
12. Bourgeois P. Scintigraphic investigations of the lymphatic system: the influence of injected volume and quantity of labeled colloidal tracer. *J Nucl Med* 2007; 48: 693-5.
13. Tsopelas C. Particle size analyses of ^{99m}Tc-labelled and unlabelled rhenium sulfide and antimony trisulphide colloids intended for application in lymphoscintigraphic studies. *J Nucl Med* 2001; 42: 467-75.
14. Uren RF, Thompson JF, Howman-Giles RB. Lymphatic drainage of the skin and breast-locating sentinel nodes. *Singapore: Harwood Academic Publishers*, 1999; 48.
15. Histopaque Product Information Sheet, Procedure 1119 *Sigma Diagnostics*, USA.
16. Kumar S, Jyoti A, Keshari RS et al. Functional and molecular characterisation of NOS isoforms in rat neutrophil precursor cells. *Cytometry Part A* 2010; 77A: 467-77.
17. Scallan JP, Huxley VH. In vivo determination of collecting lymphatic vessel permeability to albumin: a role for lymphatics in exchange. *J Physiol* 2010; 588: 243-54.
18. Tilney NL. Patterns of lymphatic drainage in the adult laboratory rat. *Anat* 1971; 109: 369-83.
19. Harrell MI, Iritani BM, Ruddell A. Lymph Node Mapping in the Mouse. *J Immunol Methods* 2008; 332: 170-4.
20. Lee SH, Bae K-H, Kim GO et al. Primo Vascular System in the Lymph Vessel from the Inguinal to the Axillary Nodes. *Evidence-Based Compl. & Altern Med* 2013; Article ID 472704:1-6.
21. Suami H, Chang DW, Matsumoto K et al. Demonstrating the Lymphatic System in Rats With Microinjection. *The Anat Rec* 2011; 294: 1566-73.
22. Engeset A, Tjötta E. Lymphatic Pathways from the Tail in Rats and Mice. *Cancer Res* 1960; 20: 613-4.
23. Saad A-H, Abdel-Gaber RA, Mahmoud HM. Histopathological study of the lymphoid organs in different species of Egyptian rats. *J Am Sci* 2013; 9: 93-105.
24. Komárek V. Gross Anatomy (Chapter 13). In: GJ Krinke (Ed). *The Laboratory Rat.* Academic Press: London, 2000.
25. Weiler M, Dixon JB. Differential transport function of lymphatic vessels in the rat tail model and the long-term effects of Indocyanine Green as a assessed with near-infrared imaging. *Front Physiol* 2013; 4 (Article 215): 1-10.
26. Tsopelas C. Recent advances in nuclear medicine: Radiopharmaceutical chemistry of agents for lymphoscintigraphy and the sentinel node biopsy (Chapter II). In: A Watanabe (Ed). *Cancer Metastasis Research*. Nova Science Publishers Inc: New York, 2008.
27. Tsopelas C. Understanding the radiolabelling mechanism of ^{99m}Tc-antimony sulphide colloid. *Appl Radiat Isot* 2003; 59: 321-8.
28. Ryan JA, Overton KW, Speight ME et al. Cellular uptake of gold nanoparticles passivated with BSA-SV40 large T antigen conjugates. *Anal Chem* 2007; 79: 9150-9.
29. Salman H, Bergman M, Bessler H et al. Hypothermia affects the phagocytic activity of rat peritoneal macrophages. *Acta Physiol Scand* 2000; 168: 431-6.
30. Rodriguez ME, Van der Pol WL, Van de Winkel JG. Flow cytometry based phagocytosis assay for sensitive detection of opsonic activity of pneumococcal capsular polysaccharide antibodies in human sera. *J Immunol Methods* 2001; 252: 33-44.
31. Shoshi A, Schotter J, Schroeder P et al. Magnetoresistive-based real-time cell phagocytosis monitoring. *Biosens Bioelectron* 2012; 36: 116-22.
32. Strzelecka-Kiliszek A, Kwiatkowska K, Sobota A. Lyn and Syk kinases are sequentially engaged in phagocytosis mediated by Fc gamma R. *J Immunol* 2002; 169: 6787-94.
33. Flannagan RS, Harrison RE, Yip CM et al. Dynamic macrophage "probing" is required for the efficient capture of phagocytic targets. *J Cell Biol* 2010; 191: 1205-18.
34. Tallon S, Lawlor AC, Connon SJ. Urea-catalyzed transthioesterification: towards a new kinetic resolution methodology. *ARKIVOC* 2011; iv: 115-26.
35. Bajic G, Yatime L, Sim RB et al. Structural insight on the recognition of surface-bound opsonins by the integrin I domain of complement receptor 3. *PNAS* 2013; 110: 16426-31.
36. Zanoni I, Ostuni R, Marek LR et al. CD14 controls the LPS-induced endocytosis of Toll-like receptor 4. *Cell* 2011; 147: 868-80.
37. Lobato-Pascual A, Saether PC, Dahle MK et al. Rat macrophage C-type lectin is an activating receptor expressed by phagocytic cells. *PLOS one* 2013; 8: e57406.
38. Rogers H, Williams DW, Feng G-J et al. Role of bacterial lipopolysaccharide in enhancing host immune response to *Candida albicans*.

Clinical & Developmental Immunology 2013; Article ID 320168: 1-9.
39. Getts DR, Terry RL, Getts MT et al. Therapeutic Inflammatory Monocyte Modulation Using Immune-Modifying Microparticles. *Sci Transl Med* 2014; 6: 219fs4.
40. Schroder K, Hertzog PJ, Ravasi T et al. Interferon-γ: an overview of signals, mechanisms and functions. *J Leukoc Biol* 2004; 75: 163-89.
41. Tollis S, Dart AE, Tzircotis G et al. The zipper mechanism in phagocytosis: energetic requirements and variability in phagocytic cup shape. *BMC Systems Biology* 2010; 4: 149.
42. Sladek Z, Rysanek D. Expression of macrophage CD14 receptor in the course of experimental inflammatory responses induced by lipopolysaccharide and muramyl dipeptide. *Veterinari Medicina* 2008; 53: 347-57.
43. Matsuura M. Structural modifications of bacterial lipopolysaccharide that facilitate Gram-negative bacteria evasion of host innate immunity. *Front Immunol* 2013; 4: article 109.
44. Flynn RJ, Mulcahy G. Possible role for toll-like receptors in interaction of Fasciola hepatica excretory/secretory products with bovine macrophages. *Infect Immun* 2008; 76: 678-84.

Photo J. Nohr, WHO 15014